# Controlled Supersaturation Precipitation of Hydromagnesite for the MgCl 2 −Na 2 CO 3 System at Elevated Temperatures: Chemical Modeling and Experiment

**ARTICLE** *in* INDUSTRIAL & ENGINEERING CHEMISTRY RESEARCH · FEBRUARY 2010

Impact Factor: 2.59 · DOI: 10.1021/ie9015073



**2 AUTHORS:**

Wenting Cheng

**7** PUBLICATIONS **83** CITATIONS

SEE PROFILE

Zhibao Li

Chinese Academy of Sciences

**67** PUBLICATIONS **604** CITATIONS

SEE PROFILE

# Controlled Supersaturation Precipitation of Hydromagnesite for the $MgCl_2-Na_2CO_3$ System at Elevated Temperatures: Chemical Modeling and Experiment

**Wenting Cheng and Zhibao Li***

*Key Laboratory of Green Process and Engineering, Institute of Process Engineering, National Engineering Laboratory for Hydrometallurgical Cleaner Production Technology, Chinese Academy of Sciences, Beijing 100190, P. R. China*

A new chemical model of supersaturation ($S$) was developed and applied to test for the precipitation of hydromagnesite [$Mg_5(CO_3)_4(OH)_2 \cdot 4H_2O$] in the $MgCl_2-Na_2CO_3$ system in supersaturated solutions over the temperature range of 50−90 °C. Based on the new model with the help of the OLI platform, the contour supersaturation of $Mg_5(CO_3)_4(OH)_2 \cdot 4H_2O$ has been exactly constructed by calculating the activity coefficients of species in unstable solutions. $Mg_5(CO_3)_4(OH)_2 \cdot 4H_2O$ crystals were identified using X-ray diffraction (XRD) analysis and scanning electron microscopy (SEM) images. It was found that the crystal properties, such as morphology, particle size distribution, filtration, and sedimentation characteristics, can be optimized by controlling the supersaturation during precipitation. With the control of supersaturation, well-developed spherical-like $Mg_5(CO_3)_4(OH)_2 \cdot 4H_2O$ crystals can grow to an average size of 30−40 $\mu$m, indicating a narrow particle size distribution, good filtration characteristics, and a high sedimentation rate. In addition, the $Mg_5(CO_3)_4(OH)_2 \cdot 4H_2O$ obtained was calcined to produce high-purity MgO at 800 °C. The size and morphology of MgO were similar to the same characteristics of the corresponding precursors.

## 1. Introduction

In precipitation processes, supersaturation ($S$) is the driving force for nucleation, growth, and agglomeration phenomena that influence the crystal properties[1] (morphology, particle size distribution, filtration characteristics, and so on.). Thus, strategies for supersaturation calculation and control are very important. It is difficult to obtain supersaturation values because activity coefficients are not always available for supersaturated and saturated solutions. Many researchers use the simple concentration-based equation $S = c_0/c_e$ (where $c_0$ is the actual concentration in solution and $c_e$ is the equilibrium concentration in solution) to calculate the supersaturation without considering nonideal solutions. In fact, supersaturation values can be obtained by experiment or thermodynamic calculation. Several studies have been carried out on the thermodynamics of supersaturated solutions by utilizing electrodynamic levitator traps.[2−5] Most recently, the supersaturation of $MgCO_3 \cdot 3H_2O$ in a supersaturated electrolyte solution was calculated using Meissner's method without considering speciation in solution.[6] Therefore, a new chemical model based on the speciation approach is required and can be potentially applied to predict supersaturation in supersaturated solutions using OLI Systems software.[7,8] Then, crystals with good qualities can be produced through the control of supersaturation during the precipitation process.

Hydromagnesite [$Mg_5(CO_3)_4(OH)_2 \cdot 4H_2O$], the most commonly available magnesium hydroxy carbonate, has now been accepted as an important mineral in geology and planetology.[9,10] It has also been widely applied in industry as a fire retardant,[11] as a filler for rubber and plastic,[12] and as a magnesium source for the preparation of other magnesium compounds.[13] Therefore, this material has been attracting much attention, and a large number of chemical methods have been developed to prepare it. For example, Mitsuhashi et al.[14] developed a procedure to prepare microtube $Mg_5(CO_3)_4(OH)_2 \cdot 4H_2O$ through the carbonation of an aqueous suspension of magnesium hydroxide with carbon dioxide over the temperature range of 35−70 °C. The influence of reaction temperature (from room temperature to 95 °C) and pH on the morphology of $Mg_5(CO_3)_4(OH)_2 \cdot 4H_2O$ in the precipitation process by the reaction of $Mg(NO_3)_2$ with $K_2CO_3$ was systemically investigated by Zhang et al.[15] Most recently, Hao et al.[16] synthesized $Mg_5(CO_3)_4(OH)_2 \cdot 4H_2O$ microrods with a surface of a "house-of-cards" structure in an aqueous solution system without using any surfactants or templates during the precipitation process. However, all of the literature reports suggest that knowledge of the preparation of $Mg_5(CO_3)_4(OH)_2 \cdot 4H_2O$ with different qualities through the calculation and control of the supersaturation is limited.

In the present work, the precipitation of $Mg_5(CO_3)_4(OH)_2 \cdot 4H_2O$ in the $MgCl_2-Na_2CO_3$ system was used as a model system. The supersaturation of $Mg_5(CO_3)_4(OH)_2 \cdot 4H_2O$ was calculated by assuming that the solution was at an unstable state: there was only liquid phase without any solid phases. Activity coefficient estimation in this new model was done using the Bromley−Zemaitis equation.[17,18] Preliminary estimations of the solubility product constant ($K_{SP}$) of $Mg_5(CO_3)_4(OH)_2 \cdot 4H_2O$ using OLI's StreamAnalyzer software package (version 2.0) and comparison with experimental values yielded poor results. However, further work was undertaken with the purpose of improving OLI's $K_{SP}$ estimation capability by adding the new parameters of $K_{SP}$ to a newly established "private" databank. Then, a new chemical model of the supersaturation of $Mg_5(CO_3)_4(OH)_2 \cdot 4H_2O$ for the $MgCl_2-Na_2CO_3$ system was developed and tested in the temperature range of 50−90 °C. $Mg_5(CO_3)_4(OH)_2 \cdot 4H_2O$ crystals with good qualities were obtained by controlling the supersaturation. Moreover, high-purity MgO was obtained from the $Mg_5(CO_3)_4(OH)_2 \cdot 4H_2O$ by calcination at 800 °C.

* To whom correspondence should be addressed. Tel.: +86-10-62551557. Fax: +86-10-62551557. E-mail: zhibaoli@home.ipe.ac.cn.

10.1021/ie9015073 
Published on Web 01/04/2010

## 2. Modeling Methodology of Supersaturation

**2.1. Equilibrium Relationships.** In $Mg_5(CO_3)_4(OH)_2 \cdot 4H_2O$-saturated electrolyte aqueous systems, two types of reactions occur: partial dissolution of $Mg_5(CO_3)_4(OH)_2 \cdot 4H_2O$ and association (speciation) of ionic species. The solid−liquid equilibria and speciation reaction equilibria involved in the $MgCl_2-Na_2CO_3-H_2O$ system are outlined below.

The solid−liquid equilibrium between $Mg^{2+}$, $OH^-$, and $CO_3^{2-}$ ions and solid $Mg_5(CO_3)_4(OH)_2 \cdot 4H_2O$ in electrolyte solutions can be described by the following dissolution reaction

$$Mg_5(CO_3)_4(OH)_2 \cdot 4H_2O(s) \leftrightarrow 5Mg^{2+}(aq) + 4CO_3^{2-}(aq) + 2OH^-(aq) + 4H_2O(aq) \quad (1)$$

The supersaturation of the solution with respect to a crystal was defined as the ratio of the activity products divided by the thermodynamic equilibrium constant (which can also be called the solubility product constant, $K_{SP}$, in solid−liquid equilibria) of the crystal

$$S = \frac{(a_{Mg^{2+}})^5(a_{CO_3^{2-}})^4(a_{OH^-})^2(a_w)^4}{K_{SP}} = \frac{(m_{Mg^{2+}})^5(m_{CO_3^{2-}})^4 m_{OH^-}^2[(\gamma_{Mg^{2+}})^5(\gamma_{CO_3^{2-}})^4(\gamma_{OH^-})^2](a_w)^4}{K_{SP}} \quad (2)$$

where $a_{Mg^{2+}}$, $a_{CO_3^{2-}}$, and $a_{OH^-}$ are the activities (mol·kg$^{-1}$) of $Mg^{2+}$, $CO_3^{2-}$, and $OH^-$, respectively, in solution; $m_{Mg^{2+}}$, $m_{CO_3^{2-}}$, and $m_{OH^-}$ are the corresponding concentrations in molality (mol·kg$^{-1}$); $\gamma_{Mg^{2+}}$, $\gamma_{CO_3^{2-}}$, and $\gamma_{OH^-}$ are the ion activity coefficients; $a_w$ is the activity of water; and the solubility product constant ($K_{SP}$) for $Mg_5(CO_3)_4(OH)_2 \cdot 4H_2O$ is expressed as

$$K_{SP} = (a_{Mg^{2+}(e)})^5(a_{CO_3^{2-}(e)})^4(a_{OH^-(e)})^2(a_{w(e)})^4 = [(m_{Mg^{2+}(e)})^5(m_{CO_3^{2-}(e)})^4(m_{OH^-(e)})^2][(\gamma_{Mg^{2+}(e)})^5 \times (\gamma_{CO_3^{2-}(e)})^4(\gamma_{OH^-(e)})^2](a_{w(e)})^4 \quad (3)$$

where $a_{(e)}$, $m_{(e)}$, and $\gamma_{(e)}$ represent the activities (mol·kg$^{-1}$), concentrations in molality (mol·kg$^{-1}$), and activity coefficients, respectively, for species when dissolution reaction 1 is in equilibrium.

Table 1 provides a list of all aqueous species considered in $MgCl_2-Na_2CO_3-H_2O$ system along with their dissociation reactions. As an example, the second dissociation of $HCO_3^-$ is given by

$$HCO_3^-(aq) \leftrightarrow H^+(aq) + CO_3^{2-}(aq) \quad (4)$$

and the thermodynamic equilibrium constant for this reaction is

$$K_{HCO_3^-} = \frac{(m_{H^+(e)}\gamma_{H^+(e)})(m_{CO_3^{2-}(e)}\gamma_{CO_3^{2-}(e)})}{m_{HCO_3^-(e)}\gamma_{HCO_3^-(e)}} \quad (5)$$

**2.2. Thermodynamic Equilibrium Constant.** The thermodynamic equilibrium constant ($K_{x,T,P}$) can be calculated from the standard Gibbs free energy of reaction $x$ at temperature $T$ and pressure $P$

$$\Delta G^0_{x,T,P} = -RT \ln K_{x,T,P} \quad (6)$$

**Table 1. Chemical Species and Their Speciation Reactions in the $MgCl_2-Na_2CO_3-H_2O$ System**

| species | dissociation reaction |
|---|---|
| $H_2O$ | $H_2O(aq) \leftrightarrow H^+(aq) + OH^-(aq)$ |
| $HCO_3^-$ | $HCO_3^-(aq) \leftrightarrow H^+(aq) + CO_3^{2-}(aq)$ |
| $MgHCO_3^+$ | $MgHCO_3^+(aq) \leftrightarrow Mg^{2+}(aq) + HCO_3^-(aq)$ |
| $MgOH^+$ | $MgOH^+(aq) \leftrightarrow Mg^{2+}(aq) + OH^-(aq)$ |
| $NaCO_3^-$ | $NaCO_3^-(aq) \leftrightarrow Na^+(aq) + CO_3^{2-}(aq)$ |
| $NaHCO_3(aq)$ | $NaHCO_3(aq) \leftrightarrow Na^+(aq) + HCO_3^-(aq)$ |
| $MgCO_3(aq)$ | $MgCO_3(aq) \leftrightarrow Mg^{2+}(aq) + CO_3^{2-}(aq)$ |
| $Mg_5(CO_3)_4(OH)_2(aq)$ | $Mg_5(CO_3)_4(OH)_2(aq) \leftrightarrow 5Mg^{2+}(aq) + 4CO_3^{2-}(aq) + 2OH^-(aq)$ |

The latter is given by the stoichiometric summation of the standard partial molal Gibbs free energy of formation of all species $y$ in the reaction

$$\Delta G^0_{x,T,P} = \sum \nu_{x,y} \Delta \bar{G}^0_{y,T,P} \quad (7)$$

Therefore, to obtain the thermodynamic equilibrium constant of a reaction, one needs to know the standard molal Gibbs free energies of formation of the reaction products and reactants as shown in eqs 6 and 7. For solid species, this can be achieved in terms of the standard Gibbs free energy of formation at the reference state and the heat capacity. For aqueous species, the revised HKF model[19−21] has been used to calculate the standard partial thermodynamic properties of any aqueous species at high temperatures up to 1000 °C and pressures up to 5 kbar. The equations[20] for the five thermodynamic properties ($\bar{V}^0$, $\bar{C}^0_P$, $\bar{S}^0$, $\Delta \bar{H}^0_{P,T}$, and $\Delta \bar{G}^0_{P,T}$) in the HKF model require the values of all seven HKF parameters ($\alpha_1-\alpha_4$, $\gamma_1$, $\gamma_2$, and $\omega$). Fortunately, numerous HKF parameters have been published for many aqueous species so far.[20,21] Recently, the HKF model was incorporated into OLI Systems software[7] with a well-designed interface and easy operation, which was actually employed in the present work. Table 2 lists the thermodynamic data of the relevant species used in the OLI software to calculate thermodynamic equilibrium constants with the aid of the HKF equation, and Table 3 lists the values of the seven HKF parameters for the relevant species. The thermodynamic equilibrium constants of all of the aqueous dissociation reactions in Table 1 were calculated by this method. However, the solubility product constants of $Mg_5(CO_3)_4(OH)_2 \cdot 4H_2O$ were calculated by the following empirical equation in the OLI software

$$\log K_{SP} = A + \frac{B}{T} + CT + DT^2 \quad (8)$$

where $A$, $B$, $C$, and $D$ are empirical parameters and $T$ is the temperature in Kelvin.

**Table 2. Thermochemical Data for the Main Species in the $MgCl_2-Na_2CO_3-H_2O$ System Used by OLI to Calculate Equilibrium Constants with the HKF Method[a]**

| species | $\bar{V}^0_{P,25}$ ($cm^3 \cdot mol^{-1}$) | $\bar{C}^0_{P,25}$ ($J \cdot K^{-1} \cdot mol^{-1}$) | $\Delta\bar{S}^0_{f,25}$ ($J \cdot K^{-1} \cdot mol^{-1}$) | $\Delta\bar{H}^0_{f,25}$ ($kJ \cdot mol^{-1}$) | $\Delta\bar{G}^0_{f,25}$ ($kJ \cdot mol^{-1}$) |
|---|---|---|---|---|---|
| $H^+$ | 0 | 0 | 0 | 0 | 0 |
| $OH^-$ | −4.18 | −137.19 | −10.711 | −229.99 | −157.3 |
| $H_2O$ | 18.1 | 75.3 | 69.95 | −285.83 | −237.19 |
| $CO_3^{2-}$ | −5.02 | −290.79 | −49.999 | −675.23 | −527.98 |
| $HCO_3^-$ | 24.6 | −35.4 | 98.45 | −689.93 | −586.94 |
| $Mg^{2+}$ | −21.6 | −22.34 | −138.1 | −465.97 | −453.96 |
| $MgCO_3$(aq) | −29.6 | −240.8 | −100.4 | −1132.1 | −998.97 |
| $MgHCO_3^+$ | 50.1 | 105.12 | −37.97 | −1164.4 | −1049.9 |
| $MgOH^+$ | | | −86.19 | −689.91 | −623.9 |
| $Na^+$ | −1.11 | 37.907 | 58.409 | −240.3 | −261.88 |
| $NaCO_3^-$ | 0.265 | −78.83 | −43.93 | −934.24 | −792.99 |
| $NaHCO_3$(aq) | 31.8 | 400.17 | 77.863 | −954.69 | −849.73 |
| $Cl^-$ | 17.8 | −123.18 | 56.735 | −167.08 | −131.29 |

[a] Data are from the Public databank of OLI.

**Table 3. Values of Seven HKF Parameters for the Main Species in the $MgCl_2-Na_2CO_3-H_2O$ System[a]**

| species | $\alpha_1 \times 10$ | $\alpha_2 \times 10^{-2}$ | $\alpha_3$ | $\alpha_4 \times 10^{-4}$ | $\gamma_1$ | $\gamma_2 \times 10^{-4}$ | $\omega \times 10^{-5}$ |
|---|---|---|---|---|---|---|---|
| $H^+$ | 0 | 0 | 0 | 0 | 0 | 0 | 0 |
| $OH^-$ | 1.2527 | 0.0738 | 1.8423 | −2.782 | 4.15 | −10.35 | 1.724 |
| $CO_3^{2-}$ | 2.8524 | −3.984 | 6.4142 | −2.614 | −3.320 | −17.19 | 3.391 |
| $HCO_3^-$ | 7.5621 | 1.1505 | 1.2346 | −2.827 | 12.940 | −4.758 | 1.273 |
| $Mg^{2+}$ | −0.8217 | −8.599 | 8.39 | −2.39 | 20.8 | −5.892 | 1.537 |
| $MgCO_3$(aq) | −19.914 | 117.08 | 140.04 | −90.26 | −4.1404 | 44.776 | 4.6779 |
| $MgHCO_3^+$ | 33.3471 | −84.003 | −272.31 | 93.352 | 30.071 | 13.0034 | 2.1447 |
| $MgOH^+$ | 2.094 | −2.6684 | 6.7988 | −2.6687 | 21.709 | −0.413 | 0.8683 |
| $Na^+$ | 1.839 | −2.285 | 3.256 | −2.726 | 18.18 | −2.981 | 0.3306 |
| $NaCO_3^-$ | 2.4059 | −1.9069 | 6.4995 | −2.7002 | 17.684 | −4.7538 | 1.787 |
| $NaHCO_3$(aq) | 6.0948 | 7.1005 | 2.9592 | −3.0725 | −153.976 | 247.65 | 0.21934 |
| $Cl^-$ | 4.032 | 4.801 | 5.563 | −2.847 | −4.40 | −5.714 | 1.456 |

[a] Values are from the Public databank of OLI.

**2.3. Ion Activity Coefficient and Water Activity Relationships.** It is clear from eqs 2 and 3 that determination of the supersaturation necessitates knowledge of the relevant ion activity coefficients and the activity of water in saturated and supersaturated solutions. There are several types of coefficient models that can be used to this end.[8,17] However, the Bromley−Zemaitis activity coefficient model[7,8] developed by Bromley[18] and empirically modified by Zemaitis[17] is used in the OLI software. This model has been successfully used for electrolytes with concentrations of 0−30 M in the temperature range of 0−200 °C;[17] hence, it is appropriate for the present system, which has concentrations of less than 3 M in the temperature range of 25−100 °C. The Bromley−Zemaitis activity coefficient model for the case of cation $i$ in a multicomponent electrolyte solution is expressed by the equation

$$\log \gamma_i = \frac{-AZ_i^2\sqrt{I}}{1+\sqrt{I}} + \sum_j \left[ \frac{(0.06 + 0.6B_{ij})|Z_iZ_j|}{\left(1 + \frac{1.5I}{|Z_iZ_j|}\right)^2} + B_{ij} + C_{ij}I + D_{ij}I^2 \right] \left(\frac{|Z_i| + |Z_j|}{2}\right)^2 m_j \quad (9)$$

where $j$ indicates all anions in solution; $A$ is the Debye−Huckel parameter; $I$ is the ionic strength of the solution; $B$, $C$, and $D$ are temperature-dependent empirical coefficients; and $Z_i$ and $Z_j$ are the cation and anion charges, respectively. $B_{ij} = B_{1ij} + B_{2ij}T + B_{3ij}T^2$ (where $T$ is the temperature, in degrees Celsius), and the other coefficients $C$ and $D$ have similar forms of temperature dependence. For the activity coefficient of an anion, the subscript $i$ represents that anion and the subscript $j$ then represents all cations in the solution. Each ion pair is described with this nine-parameter equation. The nine parameters are determined by regression of the electrolyte solution properties, such as osmotic coefficient data or solubility data.

In the case of neutral aqueous species, such as $MgCO_3$(aq), the Bromley−Zemaitis model (eq 9) cannot be used. In this case, the expression proposed by Pitzer[22] is used to obtain the activity coefficient

$$\ln \gamma_{aq} = 2\beta_{0(m-m)} + 2\beta_{1(m-s)}m_s \quad (10)$$

where $\beta_{0(m-m)}$ is the adjustable parameter for molecule−molecule interactions, $\beta_{1(m-s)}$ represents the adjustable parameter for molecule−ion interactions, and $m_s$ is the concentration of the neutral species.

Finally, for the activity of water in a multicomponent system, the formulation proposed by Meissner and Kusik[23] is adopted in OLI's thermodynamic framework

$$\log(a_w)_{mix} = \sum_i \sum_j X_iY_j \log(a^0_w)_{ij} \quad (11)$$

where $(a^0_w)$ is the hypothetical water activity of pure electrolyte $ij$ (where $i$ is an odd number for all cations and $j$ is an even number for all anions), $X_i$ represents the cationic fraction ($X_i = I_i/I_c$), and $Y_j$ represents the anionic fraction ($Y_j = I_j/I_a$).

After the calculation of the thermodynamic equilibrium constant, ion activity coefficient, and water activity, the supersaturation of $Mg_5(CO_3)_4(OH)_2 \cdot 4H_2O$ was obtained simply using eq 2.

## 3. Experimental Section

**3.1. Experimental Materials.** Chemical reagents, $MgCl_2 \cdot 6H_2O$, and $Na_2CO_3$ used in the experiments were analytical grade and were used without further purification. The water used

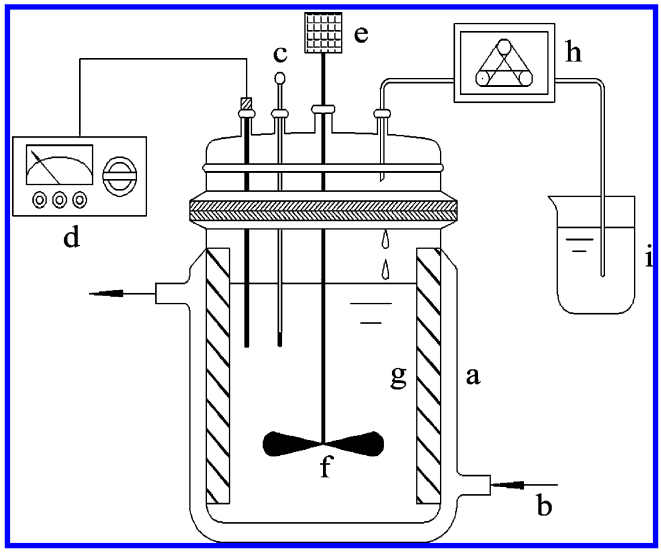


**Figure 1.** Experimental setup used in the precipitation process.

in all experimental work for solution preparation, dilution, crystal washing, and so on, was doubly distilled water (conductivity < 0.1 $\mu S \cdot cm^{-1}$).

**3.2. Homogeneous Precipitation Tests.** The experiments were performed in a 1-L double-jacketed glass reactor connected to a water circulator as shown in Figure 1. A standard volume of $MgCl_2$ located in the reactor (a) was heated to the desired temperature with circulating water (b). Solution temperature was monitored with a thermometer (c), and pH values were monitored with a pH meter (d). Upon attainment of the desired temperature, addition of $Na_2CO_3$ solution [in a beaker (i)] and stirring at 300 $min^{-1}$ were simultaneously started. Stirring was provided by a motor drive (e), and a two-blade radial impeller (f) was used. The location of the impeller and four baffles (g) attached to the lid provided uniform mixing. During the $MgCl_2-Na_2CO_3$ reaction, $Na_2CO_3$ addition by titration was done using a pump (h). When the addition procedure was completed, stirring was continued for a certain time.

At the end of each cycle, the slurry was divided into two parts. One part was filtered, washed with distilled water three times (to remove any possible ionic remnants), and finally dried in an oven at 50 °C for 10 h. A small sample from the dried magnesium carbonate hydrate was subjected to solid analysis and solubility measurements. The other part was used for the measurements of filtration characteristics, sedimentation rates, and particle size distributions.

**3.3. Measurement of Hydromagnesite Solubility.** The solubility of $Mg_5(CO_3)_4(OH)_2 \cdot 4H_2O$ in pure water was determined to obtain the solubility product constant. For this measurement, 200 mL of water was added to Erlenmeyer flasks, 250 mL in volume, that were equipped with a magnetic stirrer and capped with glass stoppers. The flasks were then immersed in a temperature-controlled water bath, and the solution was allowed to stir continuously for about 0.5 h to establish temperature equilibrium. The temperature was kept constant to within 0.1 °C. Then, excess solid [2 g of $Mg_5(CO_3)_4(OH)_2 \cdot 4H_2O$] was quickly added to the solutions in the flasks, which were tightly capped again using glass stoppers to avoid the absorption of $CO_2$. After solid−liquid equilibrium was attained (the standard equilibration time used was 6 h), stirring was stopped to allow remaining solids to settle. The supernatant solution was then withdrawn and immediately filtered using 0.22-$\mu$m Whatman Puradisc syringe filters. The clear filtrate kept in the water bath was poured into a 25-mL volumetric flask heated to the bath temperature in order to measure the density of the $Mg_5(CO_3)_4(OH)_2 \cdot 4H_2O$-saturated solution. The content of Mg was determined by chemical analysis. The solubility of $Mg_5(CO_3)_4(OH)_2 \cdot 4H_2O$ in pure water, expressed in moles per kilogram of $H_2O$, was obtained, and the results from the Mg analysis are listed in Table 4.

**Table 4. Solubility ($m_{hyd}$) and Solubility Product Constant ($K_{SP}$) of $Mg_5(CO_3)_4(OH)_2 \cdot 4H_2O$ in Pure Water at 25−100 °C**

| | | log $K_{SP}$ | | |
|---|---|---|---|---|
| $T$ (°C) | $m_{hyd}$ (mol·kg$^{-1}$) | experimental | calculated by the OLI−HKF method | calculated by OLI with the new model |
| 25 | 0.001628 | −31.9 | −57.7 | −31.9 |
| 30 | 0.001572 | −32.0 | −58.0 | −32.3 |
| 35 | 0.001413 | −32.5 | −58.4 | −32.7 |
| 40 | 0.001325 | −32.8 | −58.8 | −33.0 |
| 45 | 0.001281 | −33.0 | −59.2 | −33.3 |
| 50 | 0.001181 | −33.4 | −59.6 | −33.5 |
| 55 | 0.001126 | −33.6 | −60.0 | −33.8 |
| 60 | 0.001069 | −33.9 | −60.4 | −34.0 |
| 70 | 0.001027 | −34.1 | −61.2 | −34.3 |
| 80 | 0.0009374 | −34.5 | −62.0 | −34.8 |
| 90 | 0.0008550 | −34.9 | −62.9 | −35.2 |
| 100 | 0.0007341 | −35.7 | −63.8 | −35.9 |

**3.4. Measurement of Filtration Characteristics.** The filtration characteristics of the precipitate were measured immediately following the precipitation test to avoid any property change due to a change in temperature. Filtration was carried out using a press filter under 80 kPa of pressure and three pieces of filter paper (10−20 $\mu$m) of 9-cm diameter. A certain volume (100 mL) of slurry was placed in the filter, and the filter was immediately sealed tight. Then, a pressure of 80 kPa was introduced in the filter, and a timer was started when liquid discharged at the same time. The moment when the pressurized flow of liquid stopped, the filtration time was recorded.

**3.5. Measurement of Sedimentation Rate.** Sedimentation was carried out using a 500-mL volumetric cylinder. A certain volume (400 mL) of slurry was placed in the volumetric cylinder and kept stable for 1 h. The height of the interface between liquid and solid was recorded every 0.5 min.

**3.6. Characterization.** The structure and morphology of the synthesized samples were examined using X-ray diffraction (XRD) analysis and scanning electron microscopy (SEM). XRD (X'Pert PRO MPD, PANalytical, Almelo, The Netherlands) patterns were recorded on a diffractometer (using Cu K$\alpha$ radiation) operating at 40 kV/30 mA. A scanning rate of 0.02°/s was applied to record the patterns in the 2$\theta$ angle range from 5° to 90°. The morphology and particle size of the as-synthesized samples were examined by SEM (JEOL-JSM-6700F). Size distribution of particles was examined by a laser diffraction particle size analyze (LS-13−320). The concentration of magnesium ion in the solution was determined by titration method using standard ethylenediaminetetraacetic acid (EDTA) solution.

## 4. Results and Discussion

**4.1. Determination of $K_{SP}$ of $Mg_5(CO_3)_4(OH)_2 \cdot 4H_2O$.** The solubility of $Mg_5(CO_3)_4(OH)_2 \cdot 4H_2O$ in pure water over the temperature range of 25−100 °C was measured in this study, and the results are listed in Table 4. Values of the solubility product constant ($K_{SP}$) of $Mg_5(CO_3)_4(OH)_2 \cdot 4H_2O$ were preliminarily calculated using OLI's existing HKF model (available as software package StreamAnalyzer 2.0). Unfortunately, there was an obvious deviation between the calculated and experimental values as shown in Table 4.

With the purpose of improving the prediction capability of OLI Systems' software, in regard to the solubility product

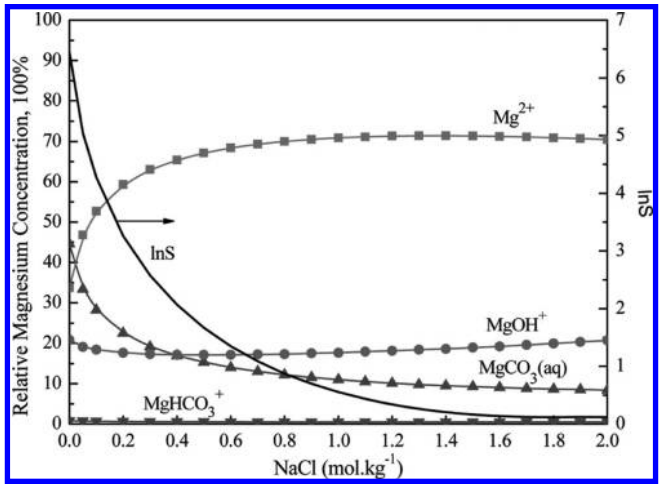


**Figure 2.** Magnesium speciation and the logarithm of the $Mg_5(CO_3)_4(OH)_2 \cdot 4H_2O$ supersaturation as functions of the NaCl concentration for a $Mg_5(CO_3)_4(OH)_2 \cdot 4H_2O$-saturated NaCl solution at 90 °C.

constant of $Mg_5(CO_3)_4(OH)_2 \cdot 4H_2O$, the experimental values for the solubility of $Mg_5(CO_3)_4(OH)_2 \cdot 4H_2O$ in pure water over the temperature range of 25−100 °C were regressed to determine new solubility product constant parameters. The empirical parameters in the solubility product constant of $Mg_5(CO_3)_4(OH)_2 \cdot 4H_2O$ (eq 8) were modified as follows

$$\log K_{SP} = -3746.96 + \frac{418668}{T} + 10.9925T - 0.01085T^2 \quad (12)$$

A new databank called "private" was created by adding the new parameters in eq 12. With the aid of eq 12 and its new parameters, the solubility product constants of $Mg_5(CO_3)_4(OH)_2 \cdot 4H_2O$ were calculated using the StreamAnalyzer 2.0 program. The predicted $Mg_5(CO_3)_4(OH)_2 \cdot 4H_2O$ solubility product constant values are given in Table 4. As can be seen, the predicted results obtained with the aid of the new chemical model are more reasonable in comparison with the experimental values than those obtained by the HKF method.

**4.2. Supersaturation and Speciation Calculations.** Having successfully modeled the solubility data of $Mg_5(CO_3)_4(OH)_2 \cdot 4H_2O$ in pure water, we proceeded to test the new model in the case of $Mg_5(CO_3)_4(OH)_2 \cdot 4H_2O$ in the $MgCl_2-Na_2CO_3$ system. The relative concentrations of magnesium species in the system containing $Mg_5(CO_3)_4(OH)_2 \cdot 4H_2O$, NaCl, and $H_2O$ and the logarithm of the $Mg_5(CO_3)_4(OH)_2 \cdot 4H_2O$ supersaturation are shown as functions of the NaCl concentration in Figure 2 at 90 °C. It can be observed that the supersaturation of $Mg_5(CO_3)_4(OH)_2 \cdot 4H_2O$ decreases with increasing NaCl concentration. The relative concentrations of $MgOH^+$ and $MgHCO_3^+$ are not significantly influenced by the NaCl concentration. However, the relative concentration of $Mg^{2+}$ consistently increases, whereas the relative concentration of $MgCO_3$(aq) decreases with increasing NaCl concentration.

**4.3. Effect of Temperature.** Precipitation is usually carried out at constant temperature and does not usually rely on cooling to produce supersaturation.[24] Temperature can strongly affect the solution precipitation process and the composition of the obtained products in the precipitation reaction of $MgCl_2$ and $Na_2CO_3$.[6] Therefore, the effect of temperature on the precipitation was investigated first. $Na_2CO_3$ solution (240 mL, 0.5 M) was added to $MgCl_2$ solution (300 mL, 0.5 M) in the temperature range of 50−90 °C, at a concentration ratio of $[Mg^{2+}]/[CO_3^{2-}] = 5/4$, allowing 2 h for addition followed by 2 h of equilibration after addition.

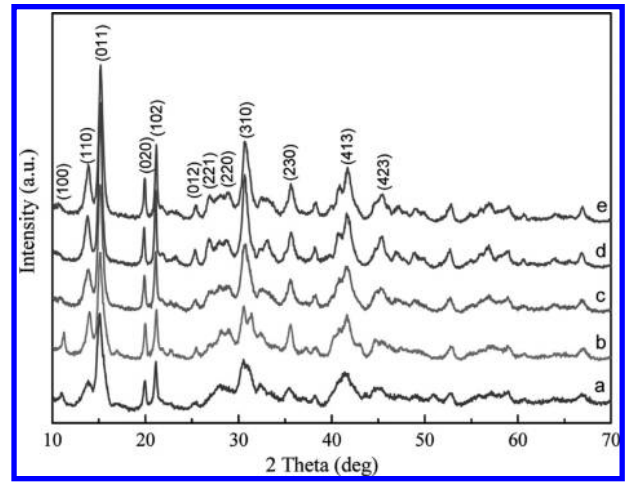


**Figure 3.** Influence of different reaction temperatures on the XRD pattern of precipitates: (a) 50, (b) 60, (c) 70, (d) 80, and (e) 90 °C.

**Table 5. Filtration Rates of $Mg_5(CO_3)_4(OH)_2 \cdot 4H_2O$ Obtained at Different Temperatures**

| temperature (°C) | filtration rate (kg·m$^{-2}$·h$^{-1}$) |
|---|---|
| 50 | 2257 |
| 60 | 2654 |
| 70 | 3987 |
| 80 | 4002 |
| 90 | 4038 |

**Table 6. Effect of Addition Time on the Sedimentation Rate and Percent Solids Density of $Mg_5(CO_3)_4(OH)_2 \cdot 4H_2O$ at a Constant Equilibration Time of 2 h Involving $Na_2CO_3$ Solution Addition at Once at 90 °C**

| titration time (h) | sedimentation rate (cm·min$^{-1}$) | solids density (%) |
|---|---|---|
| addition at once | no sedimentation | 35.1 |
| 1 | 15.3 | 52.5 |
| 2 | 18.1 | 63.2 |
| 4 | 19.4 | 64.3 |

It is evident from XRD observations (Figure 3) that precipitation at 50−90 °C results in the formation of $Mg_5(CO_3)_4(OH)_2 \cdot 4H_2O$, because the diffraction peaks are in agreement with literature values (JCPDS 25-0513). As can be seen from SEM images corresponding to the $Mg_5(CO_3)_4(OH)_2 \cdot 4H_2O$ samples prepared at different reaction temperatures (Figure 4), microtube crystals were obtained at 50 °C, whereas the precipitate became amorphous at 60 °C. When the temperature was increased to 70 °C, the amorphous particles became irregular spherical particles. The dispersion degree and average size of the spherical particles increased with increasing reaction temperature, for example, from 20−30 $\mu$m at 70 °C to 30−40 $\mu$m at 90 °C.

Figure 5 displays the particle size distributions of the $Mg_5(CO_3)_4(OH)_2 \cdot 4H_2O$ particles prepared. From 50 to 60 °C, the two curves are very irregular, and the spans, $(D_{0.9} - D_{0.1})/D_{0.5}$, are high. Above 70 °C, all curves are very close to a normal curve, and the size distribution (span) is sharpened. Therefore, the $Mg_5(CO_3)_4(OH)_2 \cdot 4H_2O$ crystals obtained at 90 °C had the largest average size and the narrowest size distribution.

The method of measuring the filtration characteristics of $Mg_5(CO_3)_4(OH)_2 \cdot 4H_2O$ was described above. Filtration rate $u$ (kg·m$^{-2}$·h$^{-1}$) is given by the equation

$$u = \frac{q}{tA} \quad (13)$$

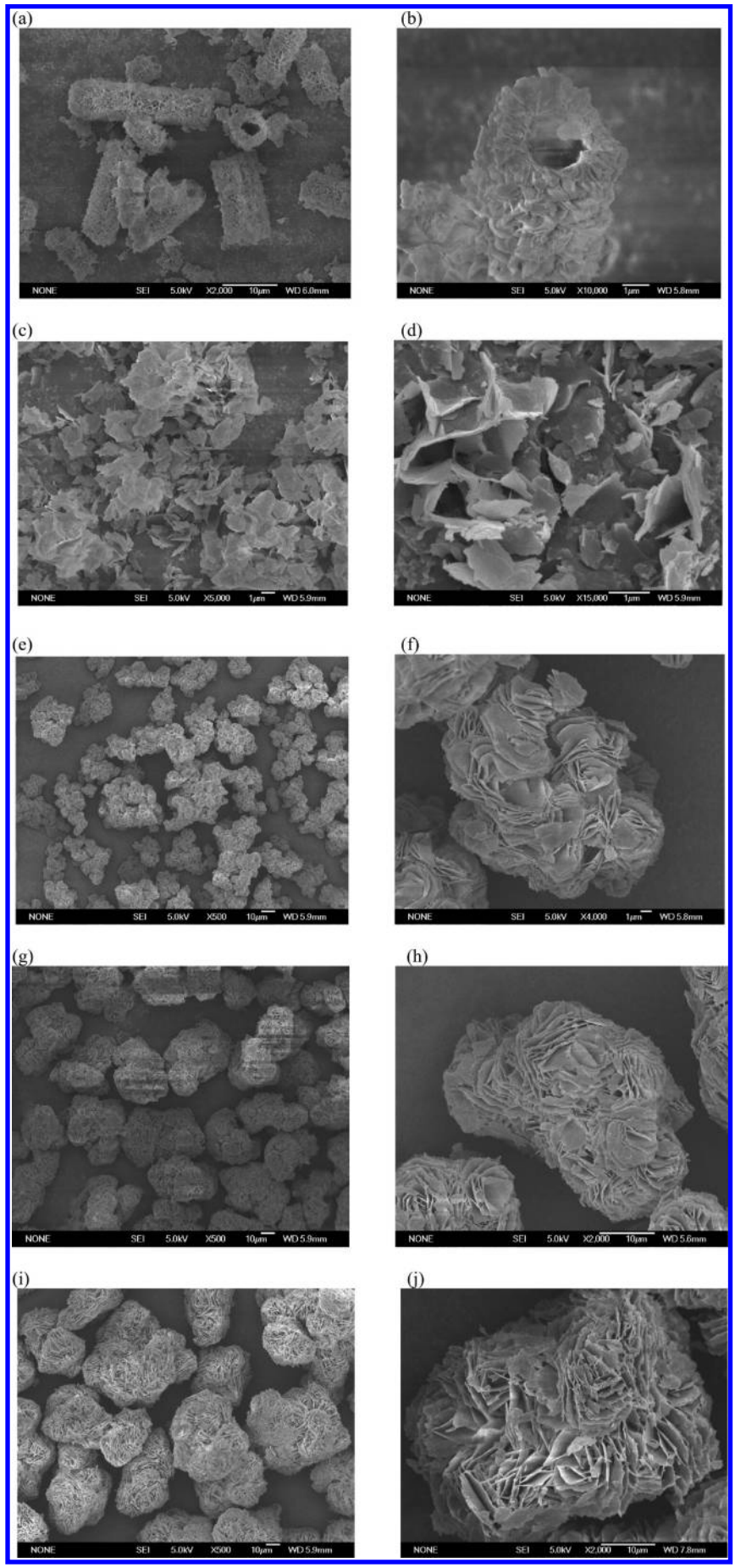


**Figure 4.** Typical SEM morphologies for the particles of $Mg_5(CO_3)_4(OH)_2 \cdot 4H_2O$ prepared at different temperatures: (a,b) 50, (c,d) 60, (e,f) 70, (g,h) 80, and (i,j) 90 °C. Note that b, d, f, h, and j are magnified images of a, c, e, g, and i, respectively.

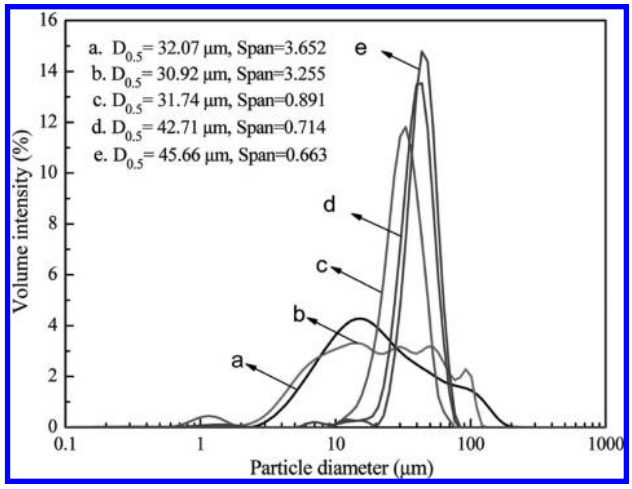


**Figure 5.** Influence of different reaction temperatures on the particle size distribution of $Mg_5(CO_3)_4(OH)_2 \cdot 4H_2O$: (a) 50, (b) 60, (c) 70, (d) 80, and (e) 90 °C.

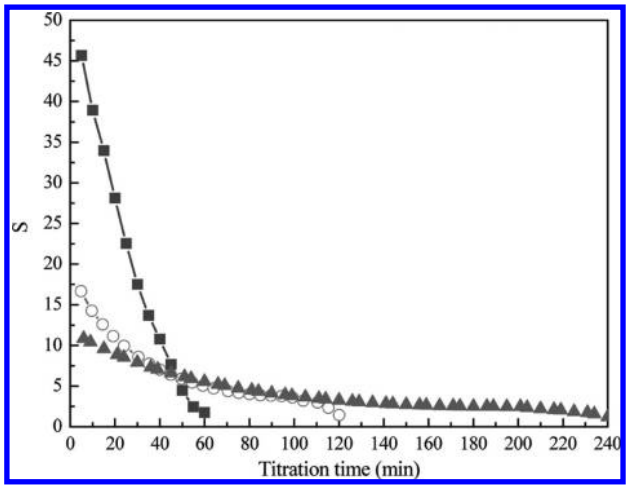


**Figure 6.** Effect of titration time on the supersaturation of $Mg_5(CO_3)_4(OH)_2 \cdot 4H_2O$ during the titration process at 90 °C: (■) 1, (○) 2, and (▲) 4 h.

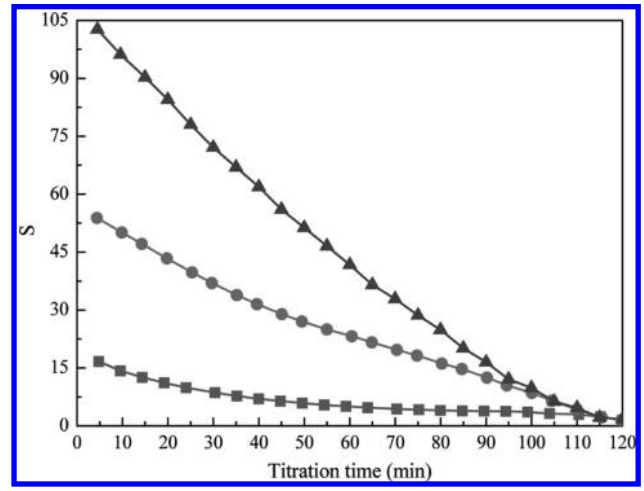


**Figure 8.** Effect of the initial concentration of $Na_2CO_3$ on the supersaturation of $Mg_5(CO_3)_4(OH)_2 \cdot 4H_2O$ at 90 °C: (■) 0.5, (●) 1.5, and (▲) 2.5 M.

where $q$ (kg) is the quality of filtrate collected from the start of the filtration to time $t$ (h) and $A$ is the filter area (63.6 $cm^2$ in this work).

As can be seen from Table 5, the experimental filtration rates of $Mg_5(CO_3)_4(OH)_2 \cdot 4H_2O$ crystals, which increase with increasing temperature, are higher than the industrial data (658−1480 $kg \cdot m^{-2} \cdot h^{-1}$).[25,26] Therefore, the experimental data are highly acceptable. Comparing Table 5 with Figures 4 and 5, it can be found that the crystals prepared at 90 °C with good morphologies and narrow size distributions exhibit good filtration characteristics.

It was decided to conduct the subsequent tests at 90 °C because of the good quality of the $Mg_5(CO_3)_4(OH)_2 \cdot 4H_2O$ crystals obtained at this temperature.

**4.4. Controlled Supersaturation by Addition Method.** $Na_2CO_3$ solution (240 mL, 0.5 M) was added to $MgCl_2$ solution (300 mL, 0.5 M) at 90 °C and a concentration ratio of $[Mg^{2+}]/[CO_3^{2-}] = 5/4$, with 2 h allowed for equilibration after the addition. Two methods of $Na_2CO_3$ addition were investigated:

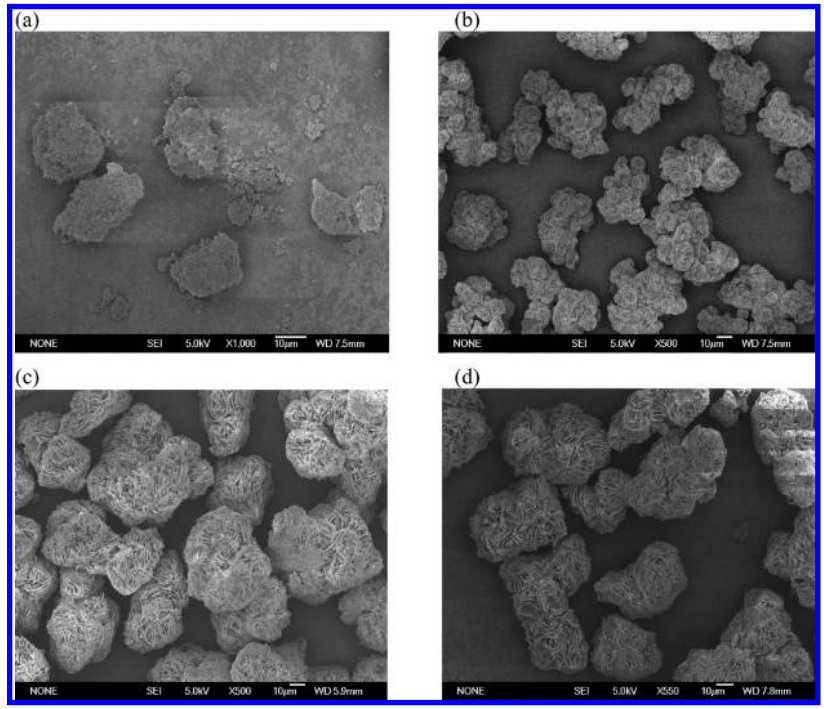


**Figure 7.** Effect of addition method on SEM morphology of $Mg_5(CO_3)_4(OH)_2 \cdot 4H_2O$ at 90 °C: (a) 0 (all of the $Na_2CO_3$ was added at once), (b) 1, (c) 2, and (d) 4 h.

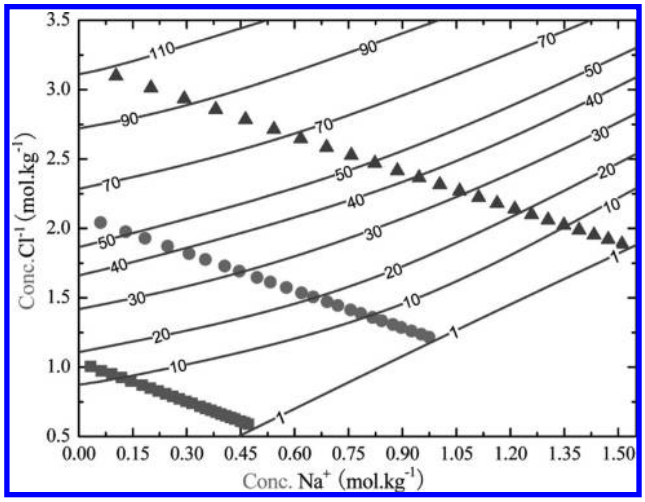


**Figure 9.** Contour lines representing supersaturation ($S$) with respect to $Mg_5(CO_3)_4(OH)_2 \cdot 4H_2O$ concentration (1−110) over the experimental range of $Na^+$ and $Cl^-$ concentrations at 90 °C. Symbols indicate solution composition during titration process at different initial concentrations of $Na_2CO_3$: (■) 0.5, (●) 1.5, and (▲) 2.5 M.

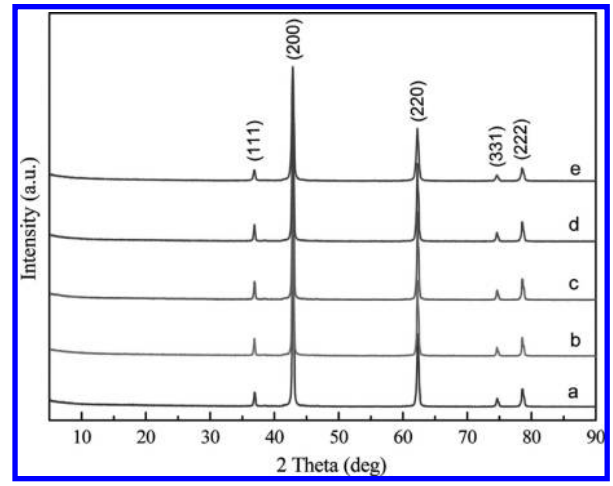


**Figure 11.** XRD patterns of MgO obtained by calcination of the corresponding precursors prepared at different reaction temperatures: (a) 50, (b) 60, (c) 70, (d) 80, and (e) 90 °C.

(1) all of the $Na_2CO_3$ was added at once, and (2) $Na_2CO_3$ was added by titration over 1, 2, and 4 h. In all cases, the XRD analysis of the crystals obtained confirmed the presence of only $Mg_5(CO_3)_4(OH)_2 \cdot 4H_2O$.

In the process of different titration methods, the supersaturations of $Mg_5(CO_3)_4(OH)_2 \cdot 4H_2O$ in $MgCl_2-Na_2CO_3$ system were calculated by the new model, and the results are shown in Figure 6. It is clear that the supersaturation of $Mg_5(CO_3)_4(OH)_2 \cdot 4H_2O$ obtained with the first addition method, $1.52 \times 10^9$, is much higher than that obtained with the second addition method. The supersaturation of $Mg_5(CO_3)_4(OH)_2 \cdot 4H_2O$ decreased with increasing addition time.

The effects of $Na_2CO_3$ addition time on the sedimentation rate and percent solids density of the resultant settled slurry are reported in Table 6. It is noticed that, when all of the $Na_2CO_3$ was added at once, a (gel-like) colloidal suspension was obtained that exhibited no settling (i.e., it had poor dewatering characteristics). However, when $Na_2CO_3$ was added by titration, the settling rate of the crystals increased with longer addition times (i.e., lower titration rates), and the percent solids density increased as well. For example, the percent solids content increased from 35.1% when all of the $Na_2CO_3$ was added at once to 64.3% with 4 h of addition. The improved results with titration can be understood upon evaluation of the crystals size and morphological characteristics in Figure 7.

As can be seen in Figure 7a, when all of the $Na_2CO_3$ was added at once, very fine needle crystals clustered together, thus explaining their gel-like behavior. This behavior can be attributed to the fact that, at extremely high supersaturation ($1.52 \times 10^9$), the primary nucleation is fast, and many crystallites with small size are produced. The two solutions cannot mix thoroughly in a very short time, which greatly decreases the

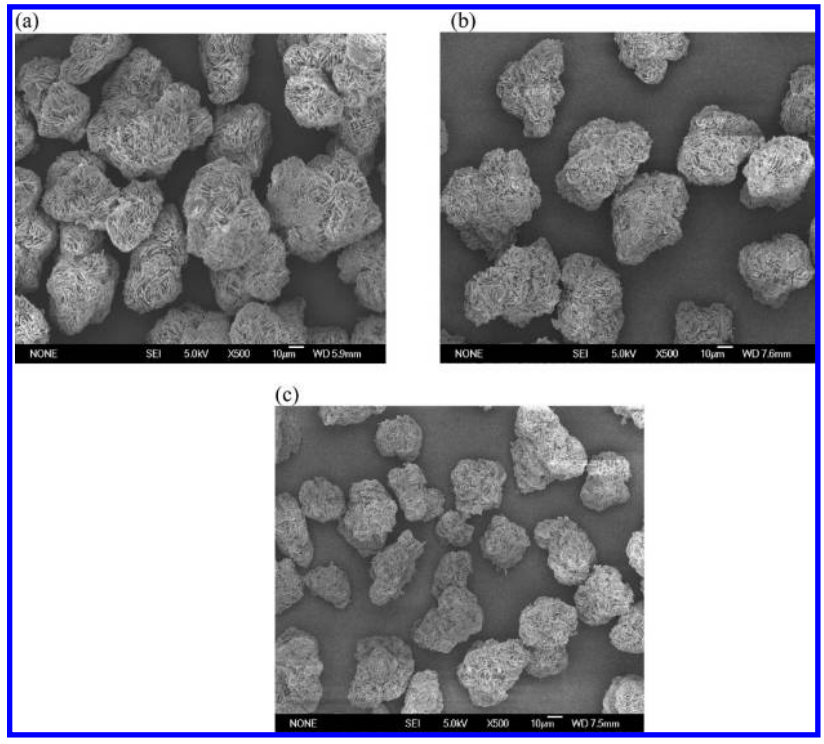


**Figure 10.** Effect of the initial concentration of $Na_2CO_3$ on the SEM morphology of $Mg_5(CO_3)_4(OH)_2 \cdot 4H_2O$ at 90 °C: (a) 0.5, (b) 1.5, and (c) 2.5 M.

**Table 7. Effect of Initial Concentration of $Na_2CO_3$ on the Sedimentation Rate and Percent Solids Density of $Mg_5(CO_3)_4(OH)_2 \cdot 4H_2O$ at 90 °C**

| initial concentration (M) | sedimentation rate ($cm \cdot min^{-1}$) | solids density (%) |
|---|---|---|
| 0.5 | 18.1 | 63.2 |
| 1.5 | 16.2 | 54.6 |
| 2.5 | 14.8 | 50.5 |

growth rate of the nuclei. Hence, particles cannot grow into larger ones and cluster together. On the other hand, irregular spherical crystals are obtained with gradual addition of the $Na_2CO_3$ by titration for 1, 2, and 4 h (Figure 7b−d). Apparently the dimensions of the crystals are smaller at shorter addition times, such as for addition for 1 h. This observation can be ascribed to the fact that, at higher superasaturation, the nucleation rate is higher than the growth rate of the nuclei[27] and particles cannot grow into larger particles. On the other hand, when the reaction occurs at lower supersaturation by titration for 2 or 4 h, the crystals grow larger. Therefore, well-developed crystals with an average size of 30−40 $\mu$m were generated by gradual titration of $Na_2CO_3$ for 2 or 4 h. Because there was not much difference in crystal properties between 2- and 4-h titration times, it was decided to conduct the subsequent titration tests with a $Na_2CO_3$ addition period of 2 h.

**4.5. Controlled Supersaturation by Different Initial Concentration.** For an engineering orientation process, it is obvious that the reagent used should be as concentrated as possible to obtain greater production of precipitate. When the initial concentration of $MgCl_2$ and $Na_2CO_3$ was 3 M, the slurry was very thick, started to adhere to the reactor walls, and was difficult to agitate. Variable initial concentrations of 0.5, 1.5, and 2.5 M $Na_2CO_3$ were investigated ($[Mg^{2+}]/[CO_3^{2-}] = 5/4$) at 90 °C.

In the process of titration at different initial concentrations of $Na_2CO_3$, the supersaturation of $Mg_5(CO_3)_4(OH)_2 \cdot 4H_2O$ was calculated by the new chemical model, and the results are shown in Figure 8. It is clear that the initial supersaturation of $Mg_5(CO_3)_4(OH)_2 \cdot 4H_2O$ increased dramatically with higher initial concentrations of $Na_2CO_3$. For example, the initial supersaturation of $Mg_5(CO_3)_4(OH)_2 \cdot 4H_2O$ was 16.7 with 0.5 M $Na_2CO_3$, whereas the initial supersaturation of $Mg_5(CO_3)_4(OH)_2 \cdot 4H_2O$ increased to 102.7 with 2.5 M $Na_2CO_3$.

The solution compositions of the precipitation experiments carried out are shown in Figure 9, where contour lines indicate conditions of constant supersaturation ratio of the solution with respect to $Mg_5(CO_3)_4(OH)_2 \cdot 4H_2O$ during the titration of $Na_2CO_3$.

The results of SEM image analysis are shown in Figure 10. As can be seen from this figure, the crystals obtained at low

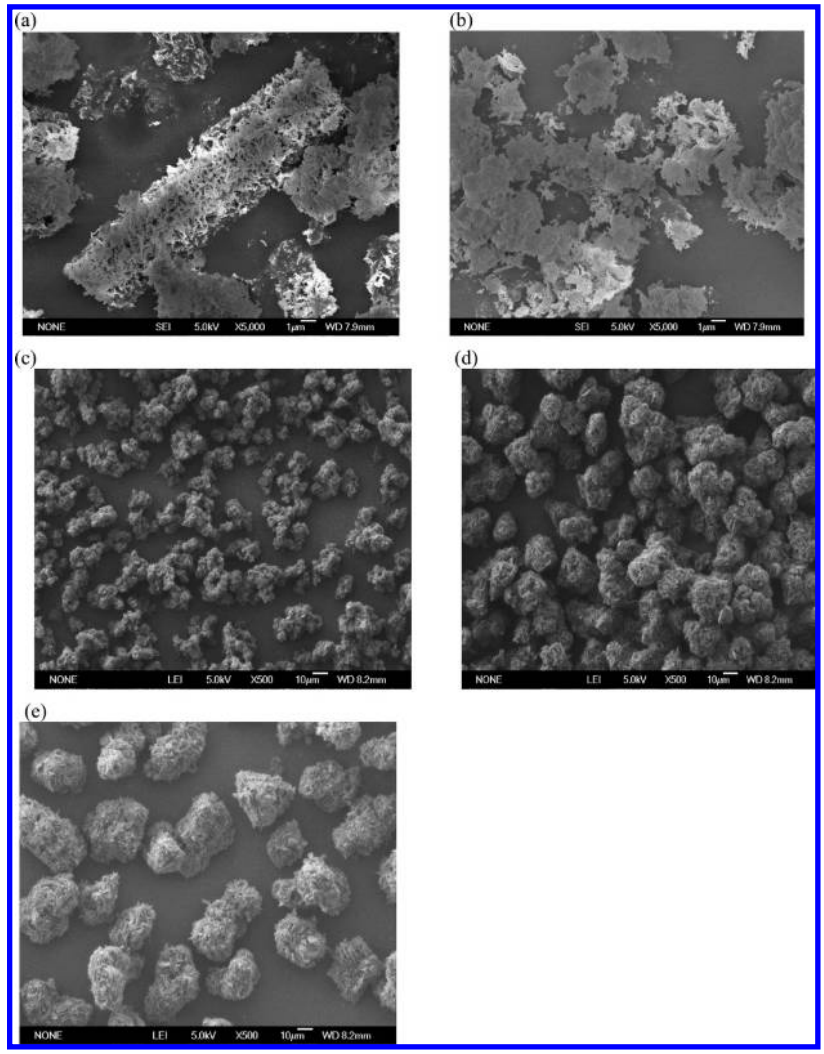


**Figure 12.** Morphology of MgO obtained by calcination of $Mg_5(CO_3)_4(OH)_2 \cdot 4H_2O$ prepared at different temperatures: (a) 50, (b) 60, (c) 70, (d) 80, and (e) 90 °C.

initial concentration of $Na_2CO_3$ (0.5 M) consist of large crystals with a 30−40-$\mu$m average size. Hence, a low concentration is beneficial for the production of crystals with a large size. The dimensions of the crystals decrease with increasing initial concentration of $Na_2CO_3$. The average size decreases to 20−35 $\mu$m for 2.5 M $Na_2CO_3$. This behavior can be attributed to the fact that, with higher concentrations of $Na_2CO_3$, higher supersaturation develops, which, in turn, gives rise to fast prime nucleation and consequent formation of small crystals.[28]

The results obtained in terms of sedimentation rate and percent solids density are reported in Table 7. It can be seen that, when the initial concentration of $Na_2CO_3$ was increased, the sedimentation rate decreased. On the other hand, the percent solids density decreased with increasing $Na_2CO_3$ concentration, namely, from 18.1 cm/min with 0.5 M $Na_2CO_3$ to 14.8 cm/min with 2.5 M $Na_2CO_3$. This behavior can be attributed to the fact that smaller crystals exhibit poorer dewatering characteristics.

**4.6. Preparation of MgO.** MgO samples were prepared by calcination of $Mg_5(CO_3)_4(OH)_2 \cdot 4H_2O$ at 800 °C for 4 h in a muffle stove.[29] Figure 11 displays the typical XRD patterns of the as-prepared MgO samples. It can be seen that the diffraction peaks of (111), (200), (220), (331), and (222) are in good agreement with the values in the literature (JCPDS 87-0651).

Figure 12 displays a set of typical SEM images of MgO obtained by calcination of the corresponding precursors prepared at different reaction temperatures. Comparing Figure 4 with Figure 12, it can be seen that the calcination treatment does not alter the surface morphology significantly and that the morphologies of MgO are similar to those of the corresponding precursors. However, the sizes of the MgO particles are slightly smaller than those of their corresponding precursors. The reason for this finding is that the MgO particles are formed more tightly by the calcination.

The solid-state reactions occurring between precursor and product during the calcination treatment are crucial in controlling both the morphology and the purity of the product. Therefore, the purities of the MgO samples have a strong relationship with those of their corresponding precursors. A certain amount of MgO produced by calcination of the corresponding precursors obtained at different conditions was dissolved in hydrochloric acid in slight stoichiometric excess. The concentration of magnesium ion in the solution was determined by titration using standard ethylenediaminetetraacetic acid (EDTA) solution. The results show that the purities of the MgO samples were all above 98%.

## 5. Conclusions

OLI Systems' StreamAnalyzer software with its default databank was used to estimate the supersaturation of $Mg_5(CO_3)_4(OH)_2 \cdot 4H_2O$ with limited success. A new set of parameters for $K_{SP}$ were determined by fitting experimental data generated by the measurement of $Mg_5(CO_3)_4(OH)_2 \cdot 4H_2O$ solubility in pure water. Finally, the databank was calibrated by adding new empirical parameters for $K_{SP}$ of $Mg_5(CO_3)_4(OH)_2 \cdot 4H_2O$. With this new model, the supersaturation of $Mg_5(CO_3)_4(OH)_2 \cdot 4H_2O$ in the $MgCl_2-Na_2CO_3$ system was exactly predicted by calculating the activity coefficients of species based on the Bromley−Zemaitis model. The modeling results indicate that the speciation-based thermodynamic model forming the basis of the OLI StreamAnalyzer program, after the improvements made to it in this work, is a good tool for calculating the supersaturation of $Mg_5(CO_3)_4(OH)_2 \cdot 4H_2O$. $Mg_5(CO_3)_4(OH)_2 \cdot 4H_2O$ crystals with different characteristics were obtained through temperature combined with supersaturation control. Extremely high supersaturation (fast addition of $Na_2CO_3$) proved counterproductive, as it yielded a gel-like fine-crystal suspension. Lower supersaturation was found to be beneficial for producing crystals with large sizes. With the control of supersaturation at 90 °C, well-developed spherical-like $Mg_5(CO_3)_4(OH)_2 \cdot 4H_2O$ crystals of 30−40-$\mu$m average size with a narrow particle size distribution, good filtration characteristics, and a high sedimentation rate can be obtained. The MgO samples obtained by calcination of $Mg_5(CO_3)_4(OH)_2 \cdot 4H_2O$ at 800 °C still maintained their corresponding precursors' morphology, and the purity of MgO was high.

## Acknowledgment

The support of the National Nature Science Foundation of China (Grant 20876161) and the National Basic Research Program of China (973 Program, 2007CB613501 and 2009-CB219904) is gratefully acknowledged.

## Literature Cited

(1) Hojjati, H.; Sheikhzadeh, M.; Rohani, S. Control of supersaturation in a semibatch antisolvent crystallization process using a fuzzy logic controller. *Ind. Eng. Chem. Res.* **2007**, *46*, 1232–1240.

(2) Cohen, M. D.; Flagen, R. C.; Seinfeld, J. H. Studies of concentrated electrolyte solutions using the electrodynamic balance. 1. Water activities for single-electrolyte solutions. *J. Phys. Chem.* **1987**, *91*, 4563–4574.

(3) Na, H.; Arnold, S.; Myerson, A. S. Cluster formation in highly supersaturated solution droplets. *J. Cryst. Growth* **1994**, *139*, 104–112.

(4) Na, H.; Arnold, S.; Myerson, A. S. Water activity in supersaturated aqueous solutions of organic solutes. *J. Cryst. Growth* **1995**, *149*, 229–235.

(5) Sun, W. M.; Myerson, A. S. In *Crystal Growth of Organic Materials*; Myerson, A. S., Green, D. A., Meenan, P., Eds.; Conference Proceedings Series; American Chemical Society: Washington, DC, 1995; p 249.

(6) Cheng, W. T.; Li, Z. B. Precipitation of nesquehonite from homogeneous supersaturated solutions. *Cryst. Res. Technol.* **2009**, *44*, 937–947.

(7) *Aqueous System Modeling Course and Workshop*; OLI Systems Inc.: Morris Plains, NJ, 2002.

(8) Rafal, M.; Berthold, J. W.; Scrivner, N. C.; Grise, S. L. Models for Electrolyte Solutions. In *Models for Thermodynamic and Phase Equilibria Calculations*; Sandler, S. I., Ed.; Marcel Dekker: New York, 1994, pp 600−685.

(9) Konigsberger, E.; Konigsberger, L. C.; Gamsjager, H. Low-temperature thermodynamic model for the system $Na_2CO_3-MgCO_3-CaCO_3-H_2O$. *Geochim. Cosmochim. Acta* **1999**, *63*, 3105–3119.

(10) Russell, M. J.; Ingham, J. K.; Zedef, V.; Maktav, D.; Sunar, F.; Hall, A. J.; Fallick, A. E. Search for signs of ancient life on Mars: Expectations from hydromagnesite microbialites, Salda Lake, Turkey. *J. Geol. Soc.* **1999**, *156*, 869–888.

(11) Toure, B.; Cuesta, J. M. L.; Gaudon, P.; Benhassaine, A.; Crespy, A. Fire resistance and mechanical properties of a huntite/hydromagnesite/antimony trioxide/decabromodiphenyl oxide filled PP−PE copolymer. *Polym. Degrad. Stab.* **1996**, *53*, 371–379.

(12) Brady, G. S.; Clauser, H. R. *Materials Handbook*; McGraw-Hill Book Company: New York, 1986.

(13) Choudhary, V. R.; Pataskar, S. G.; Zope, G. B.; Chaudhari, P. N. Surface properties of magnesium oxide obtained from basic magnesium carbonate: Influence of preparation conditions of magnesium carbonate. *J. Chem. Technol. Biotechnol.* **1995**, *64*, 407–413.

(14) Mitsuhashi, K.; Tagami, N.; Tanabe, K.; Ohkubo, T.; Sakai, H.; Koishi, M.; Abe, M. Synthesis of microtubes with a surface of "house of cards" structure via needlelike particles and control of their pore size. *Langmuir* **2005**, *21*, 3659–3663.

(15) Zhang, Z. P.; Zheng, Y. J.; Ni, Y. W.; Liu, Z. M.; Chen, J. P.; Liang, X. M. Temperature- and pH-dependent morphology and FT-IR analysis of magnesium carbonate hydrates. *J. Phys. Chem. B* **2006**, *110*, 12969–12973.

(16) Hao, Z. H.; Pan, J.; Du, F. L. Synthesis of basic magnesium carbonate microrods with a surface of "house of cards" structure. *Mater. Lett.* **2009**, *63*, 985–988.

(17) Zemaitis, J. F. Predicting Vapor−Liquid Equilibria in Multicomponent Aqueous Solutions of Electrolytes. In *Thermodynamics of Aqueous Systems with Industrial Applications*; Newman, S. A., Barner, H. E., Klein,

M., Eds.; ACS Symposium Series 133; American Chemical Society: Washington, DC, 1980; p 227.

(18) Bromley, L. A. Thermodynamic properties of strong electrolytes in aqueous solutions. *AIChE J.* **1973**, *19*, 313.

(19) Tanger, J. C., IV; Helgeson, H. C. Calculation of the thermodynamic and transport properties of aqueous species at high pressures and temperatures: Revised equations of state for the standard partial molal properties of ions and electrolytes. *Am. J. Sci.* **1988**, *288*, 19–98.

(20) Shock, E. L.; Helgeson, H. C. Calculation of the thermodynamic and transport properties of aqueous species at high pressures and temperatures: Correlation algorithms for ionic species and equation of state predictions to 5 kb and 1000 °C. *Geochim. Cosmochim. Acta* **1988**, *52*, 2009–2036.

(21) Shock, E. L.; Sassani, D. C.; Willis, M.; Sverjensky, D. A. Inorganic species in geologic fluids: Correlations among standard molal thermodynamic properties of aqueous ions and hydroxide complexes. *Geochim. Cosmochim. Acta* **1997**, *61*, 907–950.

(22) Pitzer, K. S. *Activity Coefficients in Electrolyte Solution*; CRC Press: Boca Raton, FL, 1991.

(23) Meissner, H. P.; Kusik, C. L. Aqueous solutions of two or more strong electrolytes: Vapor pressure and solubilities. *Ind. Eng. Chem. Process Des. Dev.* **1973**, *12*, 205.

(24) Sohnel, O.; Garside, J. *Precipitation: Basic Principles and Industrial Applications*; Butterworth-Heinemann: Oxford, U.K., 1992.

(25) Wang, S. H. *Handbook of Petrochemical Design*, 1st ed.; Chemical Industry Publication: Beijing, 2002; Vol. 3, p 279.

(26) McCabe, W. L.; Smith, J. C.; Harriott, P. *Unit Operations of Chemical Engineering*, 6th ed.; McGraw-Hill Education (Asia) Co.: Singapore, 2003.

(27) Mullin, J. W. *Crystallization*, 4th ed.; Butterworth-Heinemann: Oxford, U.K., 1961.

(28) Mersmann, A. Supersaturation and nucleation. *Chem. Eng. Res. Des.* **1996**, *74*, 812–820.

(29) Wang, Y.; Li, Z. B.; Demopoulos, G. P. Controlled precipitation of nesquehonite by the reaction of $MgCl_2$ with $(NH_4)_2CO_3$ at 303K. *J. Cryst. Growth* **2007**, *310*, 1220–1227.

*Received for review* September 25, 2009
*Revised manuscript received* November 22, 2009
*Accepted* December 17, 2009

IE9015073